Mechanobiology in Medicine 2 (2024) 100094

Contents lists available at ScienceDirect

Mechanobiology in Medicine

journal homepage: www.sciencedirect.com/journal/mechanobiology-in-medicine

Full length article

Strain and hyaluronic acid interact to regulate ovarian cancer cell proliferation, migration, and drug resistance

Maranda Kramer [a], Allyson Criswell [c], Kamari Marzette [a], Emerson Cutcliffe [a], Mary Kathryn Sewell-Loftin [a,b,*]

[a] Department of Biomedical Engineering, University of Alabama at Birmingham, Birmingham, AL 35294, USA
[b] O'Neal Comprehensive Cancer Center, University of Alabama at Birmingham, Birmingham AL 35233, USA
[c] Biomedical Sciences Program, Department of Clinical and Diagnostic Sciences, School of Health Professions, University of Alabama at Birmingham, USA

ARTICLE INFO

Keywords:
Ovarian cancer
Mechanobiology
Tumor microenvironment
Hyaluronic acid
CD44
Chemoresistance

ABSTRACT

The ovarian tumor microenvironment plays a critical yet is poorly understood role in the regulation of cancer cell behaviors including proliferation, migration, and response to chemotherapy treatments. Ovarian cancer is the deadliest gynecological cancer, due to diagnosis at late stages of the disease and increased resistance to chemotherapies for recurrent disease. Understanding how the tumor microenvironment (TME) interacts with biomechanical forces to drive changes to ovarian cancer cell behaviors could elucidate novel treatment strategies for this patient population. Additionally, limitations in current preclinical models of the ovarian TME do not permit investigation of crosstalk between signaling pathways and mechanical forces. Our study focused on uncovering how strains and hyaluronic acid (HA) interact to signal through the CD44 receptor to alter ovarian cancer cell growth, migration, and response to a commonly used chemotherapy, paclitaxel. Using an advanced 3D *in vitro* model, we were able to identify how interactions of strain and HA as in the TME synergistically drive enhanced proliferation and migration in an ovarian tumor model line, while decreasing response to paclitaxel treatment. This study demonstrates the importance of elucidating how the mechanical forces present in the ovarian TME drive disease progression and response to treatment.

1. Introduction

Ovarian cancer is the third most common and the most lethal gynecological cancer worldwide.[1] The most prevalent type of ovarian cancer is high-grade serous carcinoma (HGSC) which is thought to either originate in the fallopian tubes or ovaries before quickly spreading throughout the peritoneal cavity and forming metastases.[1,2] Ovarian cancer often goes undetected in early stages due to vague symptoms such as nausea, bloating, and abdominal pain [2,3]. Late-stage diagnosis means that patients present with local and/or distant metastatic disease and often the metastatic growths exhibit drug resistance.[4] Clinical interventions include primary debulking surgery to remove as much tumor mass as possible, followed by platinum-based chemotherapies including cisplatin or paclitaxel.[5] However recent work has explored neoadjuvant therapies prior to surgical removal as potentially promising for some patients.[6,7] Evidence suggests that patients develop resistance to both cisplatin and paclitaxel through off- and post-target effects of the drugs, even though the therapies target different signaling mechanisms. Furthermore, some studies indicate that the off- and post-target effectors of these drugs include the MAPK pathway and heat shock protein family, which are known to be responsive to biomechanical forces.[8] Together, this information suggests that mechanobiology of ovarian cancer may play an underappreciated role in the development of chemoresistance and disease progression. Despite ovarian cancer being such a devastating disease, little is known about the stromal components of the tumor microenvironment (TME) and the mechanical stimuli therein interact to drive ovarian cancer progression and chemoresponse. Features of the ovarian TME include extracellular matrix (ECM) proteins; a variety of secreted growth factors and cytokines that drive changes to cell behaviors; cell populations including cancer-associated fibroblasts (CAFs), immune cells, endothelial cells of nearby blood vessels as well as biomechanical forces such as shear, tensile and compressive strains.[9–11] Previous studies have shown that shear forces from ascites build-up during disease progression can lead to an increase in ovarian cancer

* Corresponding author. Department of Biomedical Engineering, University of Alabama at Birmingham, Wallace Tumor Institute, 1824 6th Avenue South, Room 630A, Birmingham, AL 35294, USA.
E-mail address: mksewellloftin@uab.edu (M.K. Sewell-Loftin).

https://doi.org/10.1016/j.mbm.2024.100094
Received 31 December 2023; Received in revised form 31 July 2024; Accepted 15 August 2024
Available online 2 September 2024

drug resistance and EMT transition.[12,13] The increased fluid pressure of the ascites can also drive increases in compressive forces.[14] Oscillatory tension has been shown to increase proliferation and migratory abilities in ovarian cancer cells;[15] these forces are generated both on the micro-scale by contractility activity of stromal cells such as CAFs as well as on the macro-scale by somatic movements.

The current study focuses on elucidating how biomechanical forces and specific matrix components of the TME interact to regulate ovarian cancer growth in the context of the malignant TME. As metastatic disease often demonstrates high levels of chemoresistance, understanding how stromal features drive such behaviors is critical to improve treatment strategies. Specifically, we are investigating micro-strains generated by stromal components; these micro-strains deform the ECM and can directly affect the cancer cells themselves. One source of the micro-strains is CAFs, which are highly contractile compared to normal fibroblasts partially due to enhanced alpha-smooth muscle actin [16–19]. Additionally, our recent work has indicated that CAFs derived from a breast cancer patient exhibit significantly larger matrix deformations compared to matched normal breast fibroblasts to drive angiogenesis.[16,17] CAFs also secrete various fibrous proteins such as collagen and fibronectin to remodel the TME and promote worse disease progression.[20,21] The tensile forces generated by CAFs in the metastatic TME may cause activation of receptors to drive mechanosignaling to promote changes in cancer cell migration, proliferation, and chemoresistance. However, little is currently known regarding if CD44 can be regulated through such mechanical stimulation.

Hyaluronic acid (HA) is a glycosaminoglycan found in the ovarian TME and its increased presence has been linked to worse prognosis of ovarian cancer, including relapse and a lower 5-year survival rate.[22,23] The source of HA in the ovarian TME can be traced to both tumor cells and CAFs.[23–25] As the disease progresses, the secreted HA from these cells is incorporated into the matrix surrounding the tumor; however, the precise mechanisms of HA synthesis and remodeling in the ovarian TME remain unclear.[11] Moreover, HA can be found in both the stroma of the TME and in the serum of cancer patients.[26] While the consensus is that stromal HA predicts a poor diagnosis, serum HA has been shown to not be a predictor of disease stage.[4,23] In addition to acting as a matrix component, HA is the ligand for cell surface receptor CD44 to promote cell signaling. Previous studies have shown that different molecular weights of HA are associated with different functional effects.[26,27] Specifically, low molecular weight HA (<1 MDa) is involved with inflammation and is pro-angiogenic while high molecular weight HA (>1 MDa) is associated with an increase in CD44 binding affinity, immunosuppressive properties, anti-inflammatory, and is anti-angiogenic.[28–32] In cancer, high molecular weight HA has been linked to proliferation, migration, and invasion through CD44 signaling.[33,34]

The binding of HA to the CD44 receptor is responsible for signaling cascades related to cell proliferation, migration, and invasion behaviors in epithelial-derived cancers.[35–37] The CD44 receptor contains a variable extracellular region with a binding domain for HA, a single transmembrane domain, and an intracellular domain 38. The variable extracellular domain is created through splice variants from different exons during the synthesis of the receptor; several variants of CD44 have been implicated in worse prognosis of breast cancer, which shares similar etiology with epithelial ovarian cancer.[39–42] The intracellular domain of CD44 can be phosphorylated at Ser706 to control activity of the receptor and subsequent signaling.[43] CD44 is upstream of various signaling pathways including MAPK, ROCK, and PI3K/Akt which are known to be mechanosensitive.[44] Through these pathways, CD44 can influence ovarian cancer progression, including proliferation, migration, and chemotherapy drug resistance.[44,45] It has also been shown that CD44 interacts with Src, which is a known mechanotransducer and plays a role in turning tension in to a biochemical signal.[46] By connecting to ankyrin and the ERM proteins (ezrin, radixin, and moesin), the intracellular domain of CD44 acts a vehicle for connecting the surrounding TME to the cytoskeleton and to regulate the Rho-ROCK pathway to control proliferation and migration.[36,47,48] Interestingly, knockout of CD44 in mouse fibroblasts shows that cells are still able to migrate at the same speed as control cells but there is a loss of directionality.[49] This suggests a potentially more complicated role for CD44 in interpreting cues from the TME to control ovarian cancer cells.

The relationship between HA and CD44 in the context of mechanotransduction has been somewhat previously explored. Studies have shown that CD44 is required for proliferation and migration in response to matrix stiffness.[37,49] Other studies suggest that CD44 may act as a mechanosensor in response to shear stress, leading to tight cell–cell junctions in the blood brain barrier.[50] These studies allude to forces and HA in the ovarian tumor microenvironment along with increased CD44 expression may lead to more aggressive cancer cell behaviors including proliferation and migration. While it is known that the HA/CD44 axis plays a major role in ovarian cancer progression, the mechanisms behind HA signaling, specifically how stromal and serum HA seemingly differentially affect ovarian cancer progression, is not fully explored. This study investigates how strain combined with HA in both 2D and 3D environments can alter CD44 expression, downstream signaling, and the subsequent functional effects including ovarian cancer cell proliferation, migration, and drug resistance.

2. Materials & methods

2.1. Cells and reagents

Our studies utilized the HGSC OVCAR-8 ovarian cancer cell line. All cells were grown in RPMI (Corning and 10-040-CM), 10% HI FBS (Gibco, 10,082-147) and 1% pen-strep (Gibco, 15,140-122). To explore the role of CD44, we generated a knockdown (KD) line, OVCAR-8-shCD44, using shRNA (Horizon Discovery). Non-modified cells are referred to as wild type (WT). All sequences were targeted to the non-variable portion of the extracellular domain of CD44 to promote knockdown of all splice variants (Supplemental Table S1). Knockdown was validated against a scramble control (shSCR) using Western blot (Supplemental Fig. S1). All modified cells were tagged with a red fluorescent protein (RFP) reporter. Modified cells were selected using 0.6 μg/mL puromycin in media. To mimic serum HA, soluble HA (SOL HA) samples received 1 MDa HA (Sigma, 41,897) supplied with media at 1 μM and fed to the cells for 48 h before lysing or fixing. To mimic stromal HA in 2D studies, HA was plated onto tissue culture plastic or FlexCell plates (PLT HA) by incubating 1 μM 1 MDa HA in HBSS for 24 h at 4 °C before aspirating and washing twice with HBSS.[51] We utilized 1 MDa HA as it is known for upregulating CD44 signaling. No HA treatment (NT) controls received HBSS alone. Cells were seeded on treated surfaces at either 5×10^5 cells/well for 6 well plates or 1×10^5 cells/well for 24 well plates. Our models of serum- and stromal-like HA do not take into account the source of HA in the TME; in other words, the ovarian cancer cells may still secrete HA, and the molecule could remain on the surface of the cells during our studies. However, shCD44 knockdown should still have inhibited responses even if HA remains on the cell surface.

2.2. Strain treatments

Tensile strain studies utilized a FlexCell FX-6000 T system to introduce controlled strains, mimicking those generated by CAFs to OVCAR-8 cells. Cells were seeded at 5×10^5 cells/well on 6 well 2D collagen I coated FlexCell plates (UF–4001C) for 24 h before being exposed to 9% elongation at 0.3 Hz for 24 h. The elongation rate corresponds to matrix deformations generated by CAFs in previous studies.[16] The rate of strain corresponds to normal respiration rates. The strain elongation and rate parameters were chosen to correspond to our previously published studies, which indicate that 9% elongation and 0.3 Hz is sufficient to cause changes in ovarian cancer cell lines OVCAR-8 and SKOV-3 related to gene regulation and metastatic spread.[12] Cells were either lysed for Western blotting or trypsinized and harvested for sequential studies in

other TME models. To test HA, the FlexCell plates received the same SOL or PLT treatments described above, with controls (NT) having only the collagen I coating.

2.3. Western blot

After 24 h culture on FlexCell plates, cells were lysed with RIPA Buffer + HALT solution (ThermoFisher, 78,441). Samples were loaded at 50 μg of total protein and run on 12% gels before transfer to PDVF membranes. Membranes were blocked in 5% BSA in TBST for 2 h at room temperature, before incubating in primary antibodies overnight at 4 °C on an orbital mixer. Membranes were washed 4X in TBST then incubated in secondary antibodies in TBST with 5% BSA (for pCD44) or 5% milk (all others) for 2hr at room temperature. Membranes were treated with ECL and Femto-ECL (100:1) (ThermoFisher 32,106 and 34,095) then imaged using a LICOR Odyssey XF system. All samples were run in triplicate on parallel membranes and analyzed via densitometry in FIJI. For information on all antibodies used, please see Table 1.

2.4. 3D microtissue models

To create highly controlled 3D TME models, a previously developed protocol using a fibrin-based matrix was followed.[16] Briefly, cells, fibrinogen (Sigma, F8630), and thrombin (Sigma, T4648) were cast into a poly(dimethylsiloxane) (PDMS) ring with 10 mm outer diameter and 8 mm inner diameter. The result is a 1 mm thick fibrin (F) gel microtissue model of the TME. HA was introduced as a soluble factor (F + SOL HA) or as a gel-embedded factor (F + GEL HA), to mimic serum or stromal HA, respectively. To create GEL + HA samples, 1 MDa HA was mixed with fibrinogen at 9:1 F:HA before addition of cells and thrombin. Total matrix protein was held constant at 10 mg/mL. Each sample was loaded with 5 × 10^4 cells, with all studies being run in triplicate. Samples were pre-treated with tensile strain as described in Section 2.2 for 24 h before loading into the microtissue model. The 3D microtissues were fixed on day 2 for analysis via immunofluorescence.

2.5. 3D microfluidic devices for migration studies

To study cell migration, an advanced 3D microfluidic device to mimic the TME was utilized.[17] Devices were synthesized with PDMS and the design includes three independent tissue chambers, or regions, in series that can be loaded with different matrix and cell populations. Each chamber has its own fluidic lines, permitting control over flow between adjacent tissues. Prior studies have indicated that this microfluidic platform creates a 3D TME model with low levels of interstitial flow (<1 μm/s) in between the chambers; in these studies, the media is provided only to the center chamber and flows outward into the side chambers. Thus, any secreted factors from the center chamber undergo convective diffusion equally into the adjacent side chambers. The full description of the model and all parameters has been previously published.[17] In some studies, the middle chamber was loaded with 2 × 10^4 cells that were either pre-treated with Strain for 24 h as previously described or No Strain controls which were cultured on FlexCell plates but received no strain stimulation; all cells were loaded in fibrin only (F Only) gels. Side chambers were loaded with fibrin only (F only) or F + HA acellular gels. Devices were fed every day in a flow configuration where media moved outward from the middle chamber into the side chambers. Systems were cultured for 7 days before fixing, permeabilizing, blocking, and staining for Ki67 and DAPI. Total migration into side chambers was quantified on day 7 via DAPI staining (WT cells) or RFP signal (shSCR and shCD44 cells). All samples were run with at least 3 replicates.

Table 1
Antibodies utilized in Western blots and immunofluorescence studies.

Antibody/Target or Stain	Source & Product ID	Western Blot Conc.	IF Conc.
CD44	Abcam, ab189524	1:2500	N/A
Ki67	Abcam, ab16667	N/A	1:1000
pCD44	Sigma, SAB4504135	1:1000	N/A
Src	Cell Signaling Technologies, 2109	1:1000	N/A
GAPDH	Cell Signaling Technologies, 2118 L	1:1000	N/A
β-Actin	Sigma, A1978	1:40,000	N/A
Ankyrin	Invitrogen, MA5-27723	N/A	1:250
Sytox	Invitrogen, S11381	N/A	1 μL/mL
Hoescht 33342	ThermoFisher, PI62249	N/A	0.5 μL/mL
Anti-mouse IgG, HRP-linked Antibody	Cell Signaling Technologies, 7076	1:2000	N/A
Anti-rabbit IgG, HRP-linked Antibody	Cell Signaling Technologies, 7074	1:2000	N/A
AlexaFluor Gt-anti-Rb 488, 555, or 647	FisherSci, A-32731; FisherSci, A-27039; FisherSci, A-21244	1:500	N/A
AlexaFluor Gt-anti-Ms 488, 555, or 647	FisherSci, A-28175; FisherSci, A-21426; FisherSci, A-21236	1:500	N/A

2.6. Magnetic bead protocols

As the FlexcCell system could not be used simultaneously with the fibrin ring or microfluidic models, we utilized a previously developed magnetic bead platform to provide concurrent mechanical strains with our HA treatments.[16] In this system, 5 μm magnetic beads were coated with thrombin before embedding in fibrin-based gels; the end result is a system where beads are effectively but not chemically crosslinked into the gels. External magnetic forces, generated by a strong magnet on an orbital rotator inside the incubator, provide stimulation to move the beads. Therefore, these beads can be considered as "pseudo-cells" that drive strains similar to those created by CAFs or the FlexCell system, but do not add confounding features such as stromal-secreted factors. The beads were loaded into all chambers of the devices, with cell loading occurring as described above. Some devices were placed over a rotating magnet (Mag) or not over the magnet (No Mag). All samples were run with at least 2 replicates.

2.7. Chemotherapy treatments and cell death analysis

Effects of chemotherapy were tested in both 3D microtissue ring models and microfluidic devices. In the 3D TME ring models, cells were seeded at 5 × 10^5 cell/well on FlexCell plates and allowed to adhere overnight before Strain treatment as described previously. After 24 h Strain (or No Strain control) treatment, cells were trypsinized and loaded into the 3D ring-based microtissue model at 5 × 10^4 cell/sample. Cells were allowed to acclimate to the 3D environment for 6 h before treatment with 5 μM paclitaxel (FisherSci, NC0918319) or vehicle (Veh, DMSO) control. The next day, the cells were stained Sytox (Invitrogen S11381) and Hoescht 33342 (Thermofisher PI62249) for 1 h at 37 °C and 5% CO_2 before receiving a media wash and imaging. For microfluidic devices, Strain was administered via the magnetic bead protocol (Section 2.6); the devices received regular cell culture media on days 1–6 and were treated with Veh or Pac on day 7 for 24 h total treatment time. After this, Styox and Hoescht were added and allowed to diffuse for 24hr; images were collected on day 9. Images were analyzed in Fiji using the Analyze Particle plugin, with dead cells normalized to total cells via Hoescht staining.

2.8. Immunofluorescence staining and image analysis

For 2D samples, cells were fixed with 10% formalin for 20 min at room temperature, permeabilized with 0.5% Tween-20 in PBS for 30 min at room temperature and blocked with 2% BSA in PBS with 0.1% Tween-

20 (called Abdil) for 1h at room temperature. Primary antibodies were diluted in Abdil and samples were incubated for 2 h at room temperature before washing in PBS +0.1% Tween-20. Secondary antibodies were diluted in Abdil at 1:500 and incubated for 2 h at room temperature. Samples were washed in PBS +0.1% Tween-20, with one wash including 1:1000 DAPI, before imaging. For all antibodies used in immunofluorescence studies and concentrations, please see Table 1. For 3D ring microtissues, a similar protocol was followed except that primary and secondary antibody incubations were at 4 °C overnight. For 3D microfluidic device staining, all incubation periods were extended to 48 h at 4 °C.[17] Images were taken with an Olympus IX83 inverted microscope at 10X magnification. A 100 μm z-stack was acquired for all 3D samples; these images were transformed using the Max Z Project feature in FIJI for analysis. Images were subject to background subtraction and thresholding before using the Analyze Particles plugin. Background subtraction and thresholding values were maintained across experimental groups; this helped minimize differences in signal-to-background ratios and ensure robust comparisons between samples. For proliferation, number of Ki67 positive cells was normalized to total cell count via nuclear staining; for ankyrin analysis, ankyrin positive area was normalized to Hoescht positive area for each sample.

2.9. Statistical analysis

All samples were run with at least 3 replicates unless otherwise noted in figure captions. To compare results, data sets were first tested for

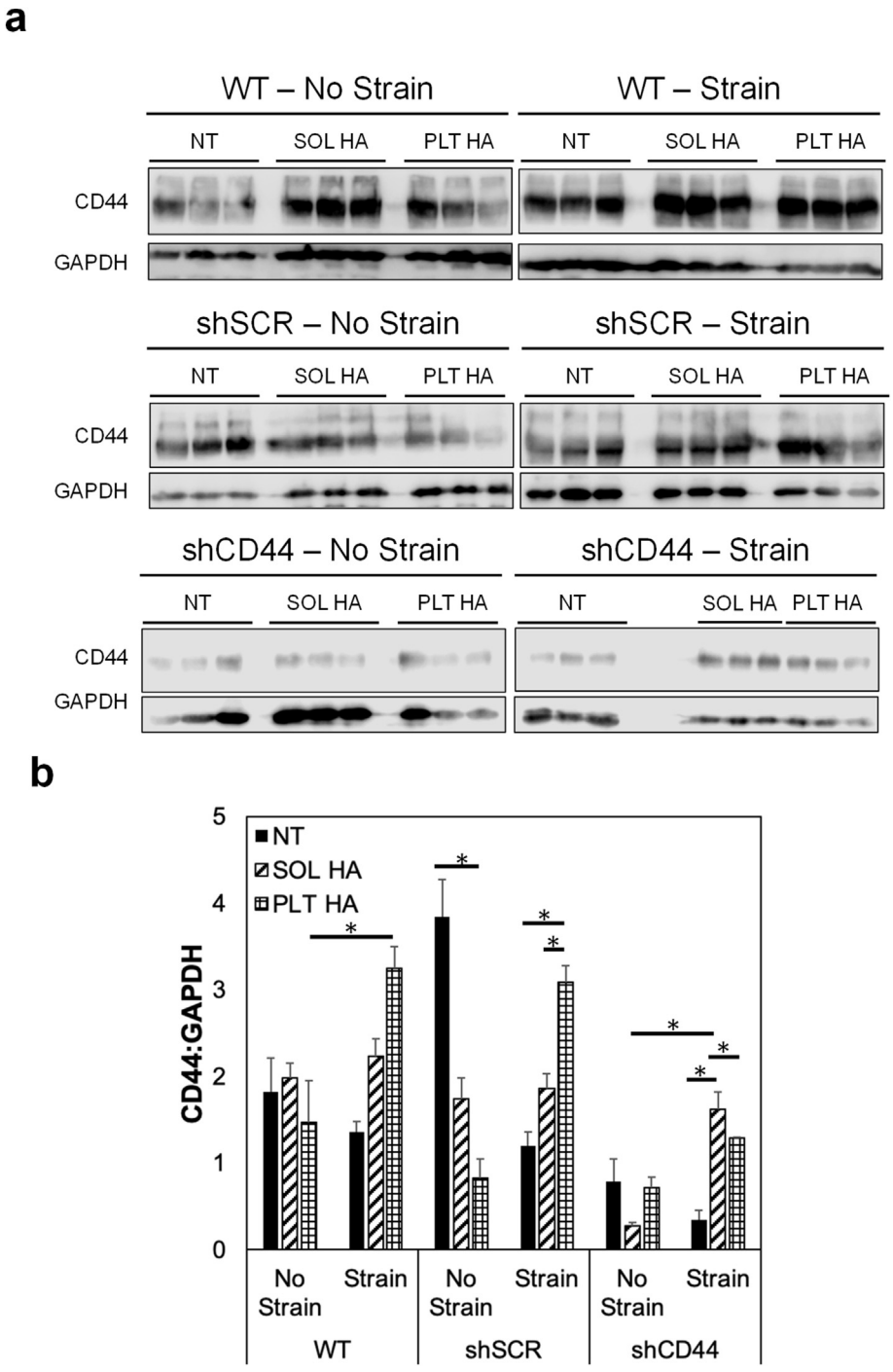

Fig. 1. CD44 Expression is Upregulated by HA and Strain Interaction. (a) Images of Western blot membranes stained for CD44 in OVCAR-8 WT, shSCR, and shCD44 cells subjected to 24 h uniaxial tensile Strain stimulation with concurrent SOL HA or PLT HA treatment. NT = No HA treatment controls (Collagen I coated FlexCell plates). No Strain samples were cultured on FlexCell plates but did not receive strain stimulation. Cropped images shown; full membranes for these images are found in Fig. S2. GAPDH included as a loading control in all samples. (b) Quantification of CD44 expression, with each band normalized to its respective GAPDH band, in Western blot samples from part (a). Data shown as average + SEM, n = 3 samples, *p < 0.05. Samples were compared using ANOVA followed by post-hoc Tukey HSD tests.

normality using the Shapiro–Wilk test. If all samples were normal, an ANOVA followed by post-hoc Tukey HSD tests were run. If any samples were non-normal, a Kruskal–Wallis analysis and post-hoc Dunn's tests were run instead. The statistical analyses for this paper were generated using the Real Statistics Resource Pack software (Release 8.9.1) [Copyright (2013–2023) Charles Zaiontz. www.real-statistics.com]. Statistical significance was considered at $p < 0.05$.

3. Results

3.1. CD44 expression is promoted by strain and HA interactions

In WT OVCAR-8 cells, concurrent Strain and SOL HA do not significantly increase normalized CD44 expression compared to NT (no HA), with or without Strain (Fig. 1a and b). Similarly, there is no increase of CD44 expression in shSCR cells treated with Strain + SOL HA compared to No Strain and Strain NT groups. In other words, our results show that cells expressing high levels of CD44 do not respond to SOL HA in the media regardless of Strain treatment. The NT samples are cultured on collagen I coated FlexCell plates to allow for direct comparison for Strain for No Strain controls in Fig. 1. Therefore, any changes observed in NT samples may represent effects of strain on collagen binding agents potentially including integrins or discoidan domain receptors, both of which have previously been implicated as mechanically sensitive.[52] In these samples the PLT HA was in addition to the collagen I on the FlexCell plates, permitting us to observe results related to stromal- or serum-like

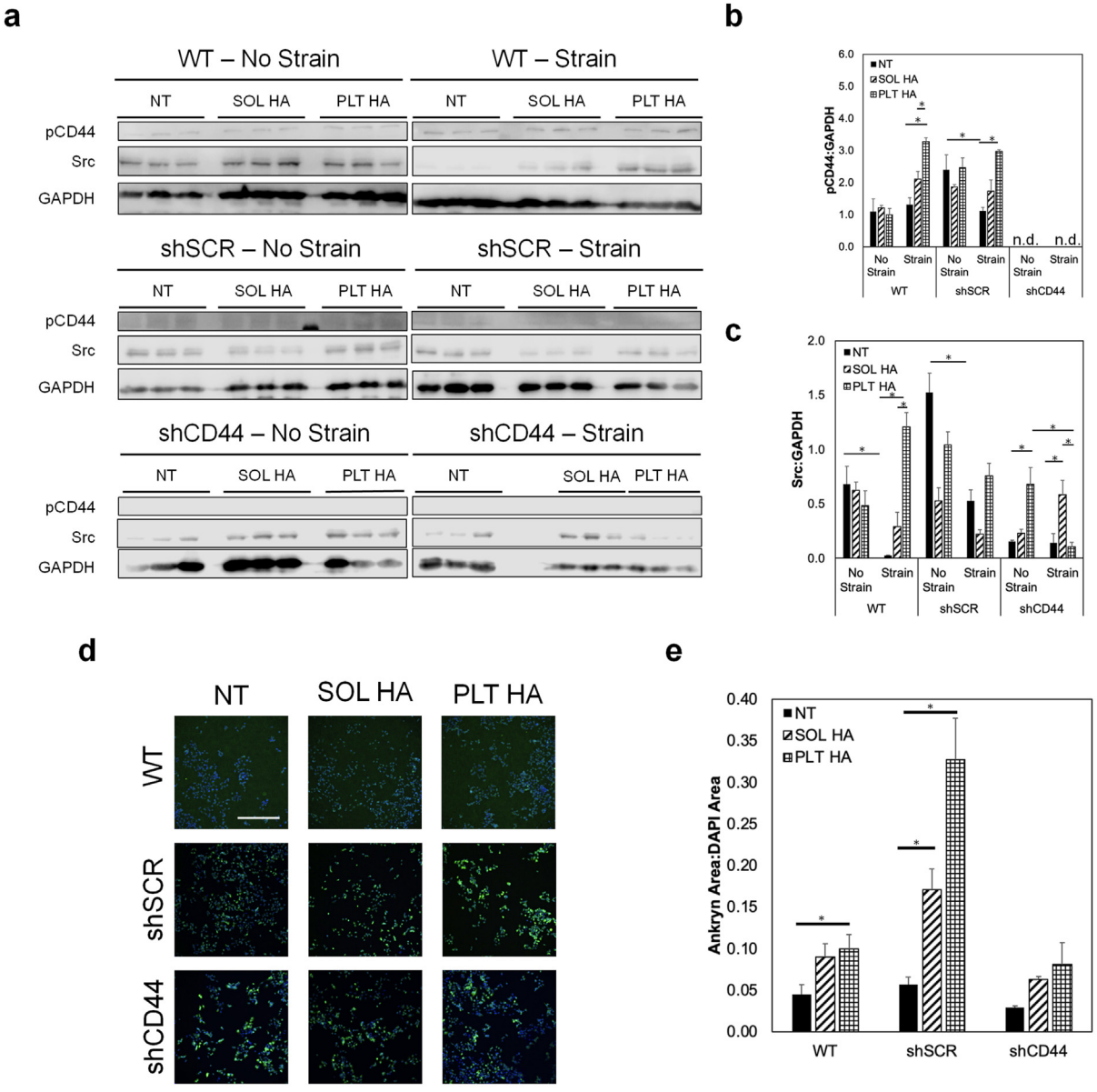

Fig. 2. CD44 Activation and Downstream Signaling is Increased with HA and Strain. (a) Images of Western blot membranes stained for pCD44 (Ser706), Src, and loading control GAPDH in OVCAR-8 WT, shSCR, and shCD44 cells subjected to 24 h uniaxial tensile strain stimulation with concurrent SOL HA or PLT HA treatment. NT = No HA treatment controls. No Strain samples were cultured on FlexCell plates but did not receive strain stimulation. Cropped images shown; full membranes in Fig. S3. (b) Quantification of normalized pCD44 expression in Western blot samples shown in part (a). Each band was normalized to its respective GAPDH band. (c) Quantification of normalized Src expression in Western blot samples shown in part (a). Each band was normalized to its respective GAPDH band. (d) Representative immunofluorescence images of OVCAR-8 WT, shSCR, and shCD44 cells treated with SOL HA or PLT HA stained for ankyrin (green) and DAPI (blue). Scale bar = 500 μm. (e) Quantification of ankyrin area normalized to DAPI area in immunofluorescence images. Data shown as average + SEM, n = 3 samples, *$p < 0.05$. Samples were compared using ANOVA followed by post-hoc Tukey HSD tests.

HA. Most notably, the Strain + PLT HA in WT cells causes an increase in CD44 expression compared to No Strain + PLT HA. A similar increase in CD44 is seen for shSCR cells with Strain + PLT HA; these cells do not increase CD44 in SOL HA or NT conditions, regardless of Strain treatment. Finally, the combination of Strain and SOL HA and PLT HA enhance CD44 expression in shCD44 OVCAR-8 cells, however these levels are still significantly lower than shSCR control samples receiving the same Strain treatments (Fig. 1b). In WT samples treated with Strain, there were no significant differences between SOL HA and PLT HA. Additionally, there is no significant difference between NT controls and SOL HA in the WT studies. Altogether, our results demonstrate that only PLT HA increases CD44 expression in Strain-treated cells compared to NT and SOL HA samples. This indicates a potential synergistic effect of stromal-like HA with strain on CD44 in OVCAR-8 cells.

To explore changes in CD44 pathway activity, we performed the Strain plus HA studies and analyzed changes in pCD44 (Ser706) and downstream Src levels (Fig. 2a and b). Both the WT and shSCR cells demonstrate significant increases in pSer706 levels when treated with concurrent Strain and PLT HA compared to Strain and NT samples. The No Strain WT and shSCR samples do not show any significant change in phosphorylated CD44 expression levels regardless of HA treatment (Fig. 2b). In other words, SOL HA treatment is not sufficient to cause increased phosphorylation of CD44 regardless of Strain treatment in in WT or shSCR cells. The OVCAR-8 shCD44 samples do not exhibit observable levels of pCD44 expression detected regardless of treatment (Fig. 2b). OVCAR-8 WT cells exhibit a significant increase in Src expression with concurrent Strain and PLT HA treatments compared to Strain with NT (no HA) (Fig. 2c). Additionally, in WT cells treated with Strain, PLT HA caused increased Src compared to Strain + SOL-HA. In shSCR control cells, studies indicate a small increase in Src with Strain + PLT HA over Strain + NT (Fig. 2c). Finally, shCD44 cells do not exhibit increased Src when treated with Strain + PLT HA, demonstrating the opposite behavior to the shSCR controls with the same treatments. In 2D studies, SOL HA and PLT HA increase the expression of ankyrin in the OVCAR-8 WT, shSCR, and shCD44 cell lines compared to uncoated tissue culture plastic (Fig. 2d and e). However, the increases in ankyrin are not significant in the shCD44 samples. Altogether, the data suggest that Strain and PLT HA can increase CD44 activation and downstream signaling.

3.2. HA in the TME increases ovarian cancer proliferation

In 2D studies, PLT HA increases the percent of proliferating cells in WT samples compared to the no HA treatment (NT) samples, while the SOL HA treated samples do not show the same increase (Fig. 3a and b). The NT samples for these studies are uncoated tissue culture plastic. The shSCR control lines demonstrate the same increase in proliferation with PLT HA and no change with SOL HA. The OVCAR-8 shCD44 samples do not have significant changes in proliferation with either SOL HA or PLT HA treatments (Fig. 3b). In the 3D TME models, Strain pre-treatment followed by F + GEL HA treatment significantly increases the percent of proliferating cells in the WT compared to Strain F Only samples (Fig. 3d). However, the Strain pre-treatment plus SOL HA does not increase Ki67 staining compared to the F Only samples (Fig. 3d). This

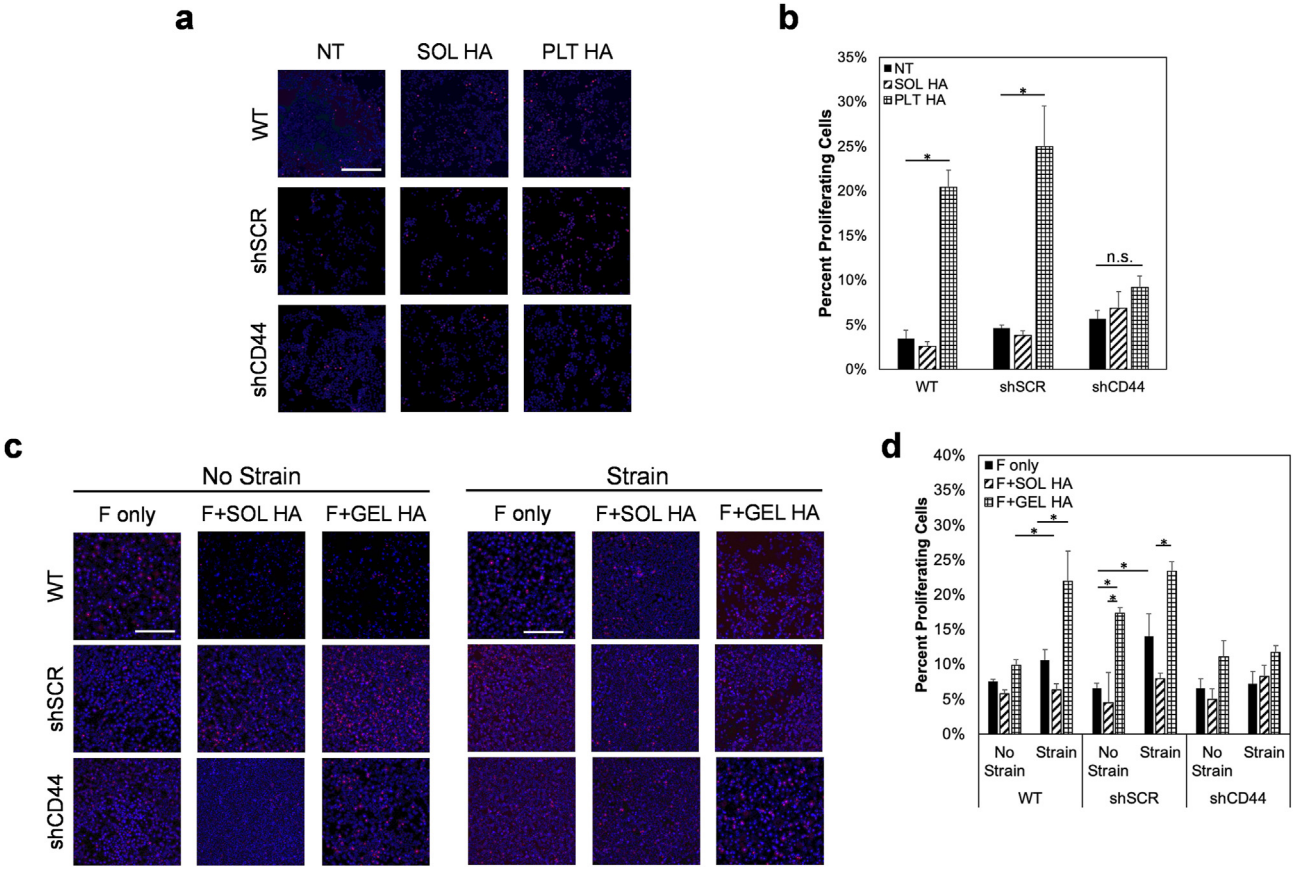

Fig. 3. HA and Strain Increase Proliferation in Ovarian Cancer Cells. (a) Representative immunofluorescence images of OVCAR-8 WT, shSCR, and shCD44 cells in 2D treated with SOL HA or PLT HA stained for Ki67 (red) and DAPI (blue). NT is no HA control. Scale bar = 500 μm. (b) Quantification of Ki67 positive cell count normalized to DAPI cell count in immunofluorescence samples. (c) Representative immunofluorescence images of OVCAR-8 WT, shSCR, and shCD44 cells treated with a 24 h Strain pre-treatment before being grown in 3D microtissue ring models with F + SOL HA or F + GEL HA. F Only is fibrin control. Scale bar = 500 μm. Images shown as Max Z intensity projection. (d) Quantification of Ki67 positive cell count normalized to DAPI cell count in immunofluorescence samples. Data shown as average + SEM, n = 3 samples, *p < 0.05. Samples were compared using ANOVA followed by post-hoc Tukey HSD tests.

indicates that the presence of HA in the matrix, but not as a media supplement, is sufficient to increase proliferation the WT cells after Strain treatment. OVCAR-8 shSCR samples demonstrate a significant increase in proliferation in the F + GEL HA environment with both No Strain and Pre-Strain treatment compared to their respective F-Only samples (Fig. 3d), further supporting that matrix or stromal-like HA with Strain is sufficient for enhancing cell growth in our 3D TME models. Finally, shCD44 cells show no significant changes in proliferation with Strain pre-treatment, F + SOL HA, or F + GEL HA (Fig. 3d).

3.3. HA and strain increase resistance to chemotherapy

To study chemoresponse, we performed Strain pre-treatment on ovarian cancer cells prior to embedding them in 3D TME models and treating with a first line chemotherapy, paclitaxel (Fig. 4a). In the OVCAR-8 WT there is an increase in cell death in response to paclitaxel (Pac) in F Only gels compared to the Veh controls (Fig. 4b and c). Moreover, SOL HA and GEL HA both decrease cell death compared to F Only, Pac treated WT cells. This demonstrates that the HA in these models, in combination with Strain pre-treatment, is protective against Pac treatment. OVCAR-8 shSCR cells that received a Strain pre-treatment had a significant increase in cell death when treated with Pac in F Only gels compared to the Veh (Fig. 4d). The Strain pre-treatment and GEL HA models showed decreased cell death in response to Pac compared to Strain F Only samples for shSCR cells, suggesting the combination of Strain and GEL HA is protective compared to F Only (Fig. 4d). For shSCR cells that did not receive strain (No Strain controls) and were cultured in GEL HA samples, there is no change in cell death between Veh and Pac groups; this suggests that stromal-like HA alone is protective against Pac treatment (Fig. 4d). The OVCAR-8 shCD44 cells show an increase in cell death with Pac treatment compared to the Veh controls with Strain pre-treatment in the F + GEL HA matrix (Fig. 4d). Moreover, in shCD44 samples, Strain pre-treatment is protective against Pac treatment in F Only gels as well. Taken together, our results indicate that interactions of Strain and stromal-like HA potentially signal through CD44 to control response to Pac treatment. Both shSCR and shCD44 cells treated with Strain and GEL HA had a slight increase in cell death for Veh treated samples compared to No Strain and F Only controls (<5%); this difference was not statistically significant, which suggests that Strain and GEL HA alone do not cause significant cell death.

3.4. Strain and Pac increase ankyrin and proliferation levels

In 3D WT samples, PLT HA increases ankyrin expression regardless of Strain treatment compared to NT (no HA) controls (Fig. 4e and f). In most cases, Pac treatment increases ankyrin in WT cells compared to Veh regardless of Strain or HA treatment. Increases in ankyrin are seen in shSCR samples with Pac treatment versus Veh controls, for all combinations of Strain and HA treatments. The shCD44 cells treated with Pac and PLT HA do not have the same increases in ankyrin expression (Fig. 4f). This suggests the low levels of CD44 are not sufficient after Strain and PLT HA stimulation to increase ankyrin levels. OVCAR-8 WT cells saw significant increases in proliferation after Pac treatment when exposed to Strain pre-treatment for both NT (no HA) and PLT HA samples (Fig. 4g). The results demonstrate that Strain pre-treatment is sufficient to increase proliferation in response to chemotherapy in these cells when in the presence of stromal-like HA. Finally, while neither shSCR or shCD44 cells showed significant differences in proliferation regardless of Pac, Strain, and HA treatments, it is notable that the chemotherapeutic did not suppress cell growth in these cells. While there is some increase in ankyrin in the shSCR cells compared to WT samples in NT conditions, we believe this may potentially be due to the shRNA modification process affecting ankyrin expression. Alternatively, other transmembrane receptors that are mechanosensitive have recently been shown to regulate ankyrin as well, so our shSCR control results may represent these off-target effects.[53] The somewhat increased levels of ankyrin in shCD44 cells compared to shSCR cells, regardless of Strain or PLT HA treatment, in Fig. 4f could be due to compensatory mechanisms of cells due to the decreased activity of CD44.

3.5. HA in the TME promotes migration

After 7 days in the microfluidic devices, our data indicate that the OVCAR-8 WT, shSCR, and shCD44 cells preferentially migrate towards the side chambers containing F + GEL HA compared to the F Only side (Fig. 5a,b,d,e). In other words, HA in the matrix as a stromal component corresponds to increased ovarian cancer cell migration potential. Some of this may be due to increased proliferation in these chambers (Fig. 5c); however, this result still demonstrates that stromal HA in the 3D TME model represents more aggressive disease compared to F Only side chambers. Pre-treatment with Strain did not influence the ability of the WT cells to migrate. While shSCR and shCD44 cells show increased migration in response to Strain pre-treatment into F + GEL HA matrices compared to F Only, there were no statistical differences in these samples (Fig. 5 d,e). Notably, these studies represent the mechanical memory of ovarian cancer cells, as they were sequentially pre-treated with Strain then embedded in the 3D TME models. To further explore how concurrent Strain and HA drive changes to ovarian cancer cell behaviors, we adapted to a pseudo-cell model to induce strains in the TME models.

3.6. Concurrent strain and HA promote more directed migration and increase proliferation

OVCAR-8 WT cells that received concurrent Strain treatment (with magnetic beads and a rotating magnetic force) only migrated into the F + HA side chamber and not F Only (Fig. 6a and b). This preferential migration is observed in both Veh and Pac treated cells. Our data also show that WT cells without the concurrent Mag Strain migrated towards the F + HA side chamber and minimally to F Only gels. While no statistical differences in cell death in response to Pac are seen in our results, there is a trend that Mag Strain decreases cell death in F + HA regions compared to middle chambers (Fig. 6c and d); there is no observed cell death in the F Only chambers, as no cells migrated into these regions. For WT cells, the Mag Strain treatment promoted more proliferation in the F + HA chambers versus No Mag Strain in the same matrix (Fig. 6f). The OVCAR-8 shSCR cells also preferentially migrated towards F + HA chambers rather than F Only, for all Veh treated groups regardless of Mag Strain stimulation (Fig. 7a–c). When treated with Pac, the preference in migration direction for control shSCR cells was maintained, even though overall migration was suppressed. However, the shCD44 samples did not show the same preference, regardless of Mag Strain or drug treatment (Fig. 7b and c). The shSCR No Mag Strain samples in the F + HA side chamber responded to Pac treatment with increased cell death in all chambers compared to Veh controls, while those that did receive the Mag Strain did not respond to the drugs (Fig. 7d). Similarly, the shCD44 samples treated with Pac showed decreased cell death when stimulated with Mag Strain compared to No Strain controls. Altogether, our results demonstrate that the role of matrix HA and CD44 is modulated by strains within the TME and this interaction drives changes to drug response and migration behaviors.

4. Discussion

The presence of HA in the ovarian TME has been shown to have conflicting roles for predicting prognoses. Specifically, stromal HA predicts a lower 5-year survival rate while serum HA levels do not correlate with disease stage. These conflicting results are evidence of our need to enhance our understanding of the ovarian TME and its role in disease progression. Our studies aimed to investigate the relationship between HA and strain on ovarian cancer cell behaviors through CD44 mechanosignaling in both 2D and 3D microtissue models. Specifically, we sought to elucidate how stromal versus serum HA differentially activates

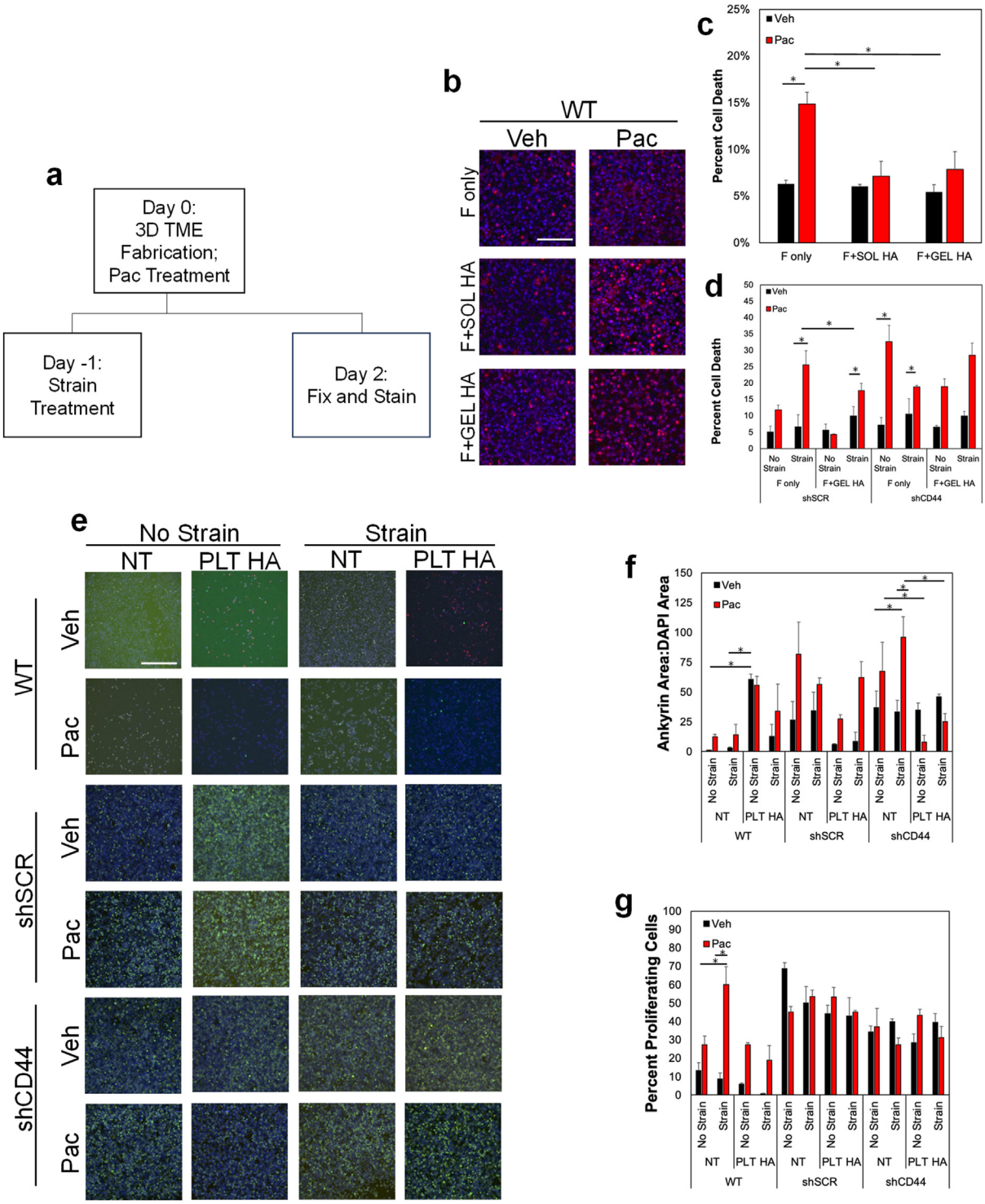

Fig. 4. Hyaluronic Acid Decreases Chemosensitivity in Ovarian Cancer Cells. (a) Timeline depicting experimental setup for parts (b) and (c). (b) Representative images of Sytox staining of OVCAR-8 WT cells grown in 3D F only, F + SOL HA and F + GEL HA gels and treated with 5 μM paclitaxel. Sytox shows dead cells (false colored - red); Hoescht nuclear stain (blue). Scale bar = 500 μm. (c) Quantification staining for Sytox in OVCAR-8 WT cells treated with Pac or Veh, showing dead cell count normalized to total cell count in immunofluorescence samples. (d) Quantification of Sytox staining for OVCAR-8 shSCR and shCD44 cells with Strain pre-treatment in F Only and F + GEL HA treated with 5 μM Pac or Veh. No Strain samples were cultured on FlexCell plates but did not receive strain stimulation prior to transfer into 3D microtissues. (e) Representative images of 2D OVCAR-8 WT, shSCR, shCD44 cells with Strain pre-treatment, with NT (No HA) or PLT HA, treated with 5 μM Pac or Veh before fixing and staining for Ki67 (green), ankyrin (red), and DAPI (blue). Scale bar = 500 μm. (f) Quantification of ankyrin positive area normalized to DAPI area in immunofluorescence samples. (g) Quantification of Ki67 cell count normalized to DAPI cell count in immunofluorescence samples. Data shown as average + SEM, n = 3 samples, *$p < 0.05$. Samples were compared using ANOVA followed by post-hoc Tukey HSD tests.

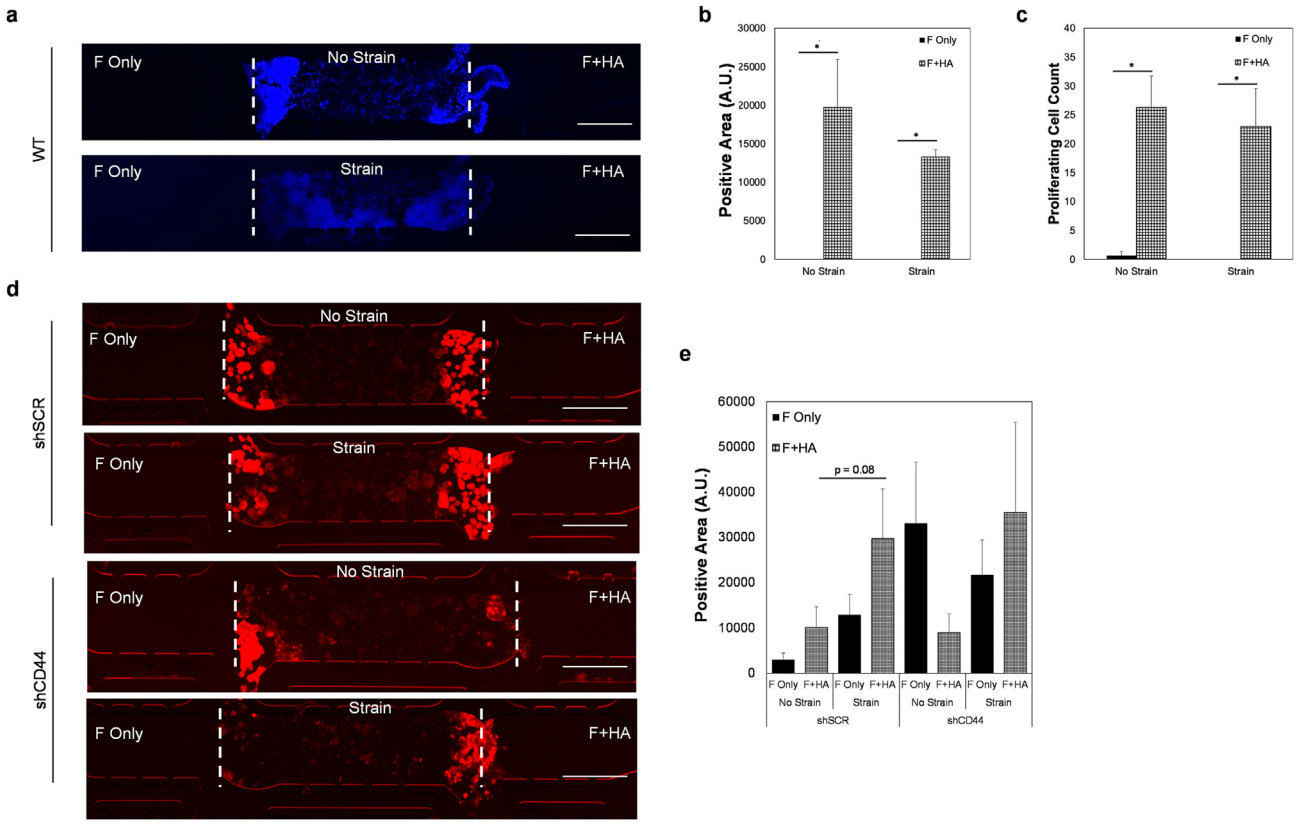

Fig. 5. Stromal HA Promotes Migration in 3D Ovarian TME Models. (a) Representative images of DAPI staining of OVCAR-8 WT cells cultured in 3-chamber TME microfluidic devices. Samples either received Strain pre-treatment (24 h) or No Strain (on non-strained FlexCell plates) prior to loading in Fibrin gels in the middle chamber of devices. Insets indicate side chamber matrix composition. White dashed lines indicate interfaces of adjacent chambers. Scale bar = 500 μm. (b) Quantification of DAPI positive area in side chambers from experiment shown in part (a). (c) Quantification of Ki67 positive cells in side chambers with different matrix compositions from part (a). (d) Representative images of RFP reporter of OVCAR-8 shSCR or shCD44 cells cultured in 3-chamber TME microfluidic devices. Samples either received Strain pre-treatment (24 h) or No Strain (on non-strained FlexCell plates) prior to loading in Fibrin gels in the middle chamber of devices. Insets indicate side chamber matrix composition. White dashed lines indicate interfaces of adjacent chambers. Scale bar = 500 μm. (e) Quantification of RFP positive area in side chambers for experiment shown in part (d). Data presented as average + SEM, n = 3 samples, *p < 0.05. Samples were compared using Kruskal-Walls followed by post-hoc Dunn's tests.

CD44 signaling with strain stimulation to regulate ovarian cancer proliferation, migration, and chemoresponse. Furthermore, we wanted to highlight that the presence of HA in the TME as a stromal matrix component may provide both mechanical and biochemical stimulation to the CD44 receptor to promote activation and downstream signaling. HA can interact with ovarian cancer cells in two different presentations, as a stromal component present in the matrix or as a serum or ascites component, free floating but still available to bind to circulating tumor cells. We modeled serum HA using solubilized HA provided with media to the cells. Stromal HA was modeled either as PLT or GEL presentations. To mimic strains in the TME, like those generated by CAFs, we utilized both a FlexCell system and a magnetic bead "pseudo-cell" model; these studies provided strains without confounding effects of stromal secreted factors. The variety of configurations allowed us to specifically investigate interactions of strain and/or HA on CD44 and subsequent cell behaviors, uncovering a specific synergistic interaction of strain and HA on CD44 signaling.

All cells demonstrated significant increases in CD44 expression only when treated with both strain and PLT HA in 2D studies (Fig. 1b). We believe our scramble controls (shSCR) cells express higher levels of CD44 compared to WT cells potentially due to the process used to modify the cells. These cells are treated with lentivirus to introduce the shRNA knockdown and selected using puromycin, which could potentially put the cells into a stress state. There is recent work suggesting that the puromycin resistance cassette can alter off-target sites including those related to differentiation and metabolic behaviors.[54,55] As this is a widely used selection mechanism for shRNA work, we have taken care to compare our shCD44 to shSCR and to not compare the modified lines with the WT samples. In the knockdown line, the initial expression levels of CD44 were roughly ~25% compared to the scramble control line (Fig. S1), but these cells also exhibited increased CD44 levels when stimulated with Strain and PLT HA. Moreover, while the shRNA knockdown was targeted to a conserved sequence across all CD44 variants, it is possible that the strain and/or PLT HA conditions enhances expression of a specific variant of CD44. Investigation of specific CD44 isoforms was beyond the scope of the current project. Altogether, the data suggest that conditions with higher levels of strain between the ligand and receptor created an increase in CD44 expression.

Next, we evaluated how these changes in CD44 expression altered activation and the regulation of downstream proteins. Concurrent Strain and PLT HA also increased the amount of phosphorylated CD44 in WT and shSCR cells (Fig. 2b). While low levels of CD44 are observed in the shCD44 samples treated with Strain (Fig. 1a), there was no detectable level of pCD44 in these same samples (Fig. 1b). We cannot state for certain that no activation of CD44 occurred in the knockdown cells, just that the levels are significantly lower compared to the shSCR cells of the same treatments (Fig. 2). Notably, phosphorylation of CD44 has been reported to be important for melanoma cell proliferation but not necessarily cell migration.[56,57] This potentially explains our additional results, where changes in shCD44 proliferation and migration were not always statistically different than shSCR samples. Importantly, the SOL HA treatments, even combined with Strain did not cause the same increases

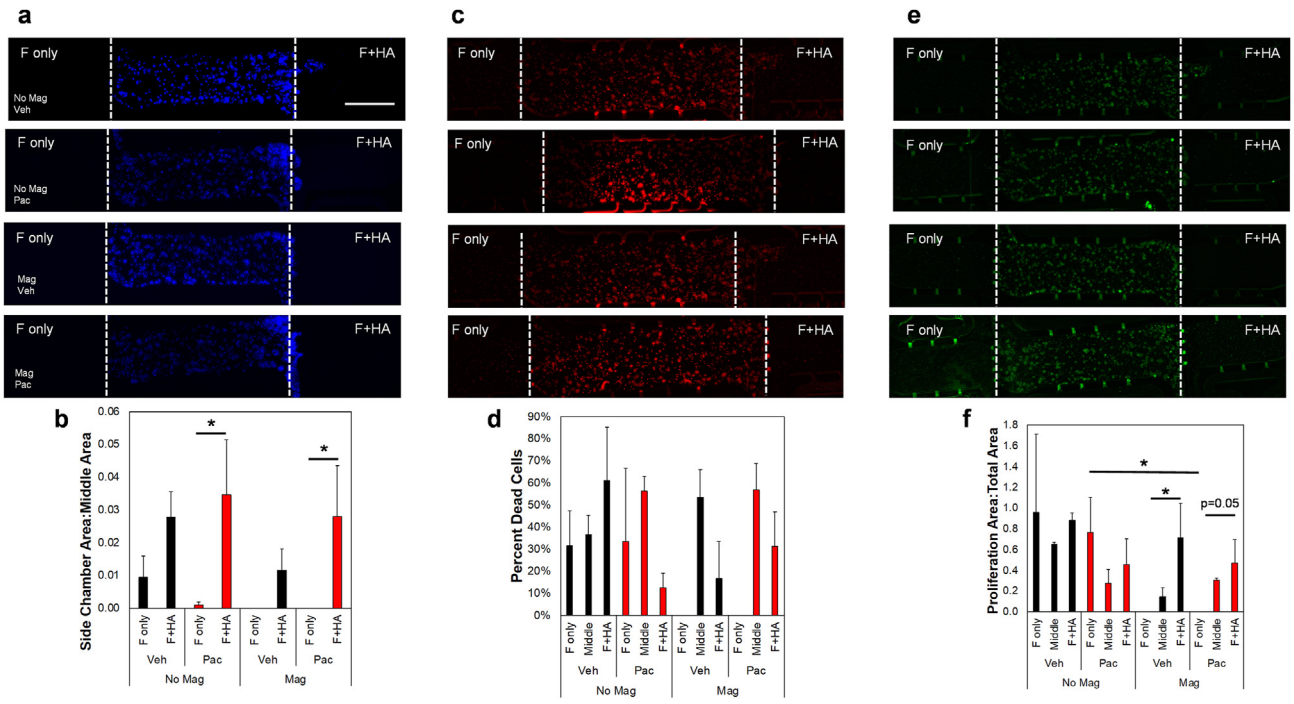

Fig. 6. Concurrent Strain and Matrix HA Increase OVCAR-8 Migration and Proliferation. (a) Representative images Hoescht staining of OVCAR-8 WT cells cultured in 3-chamber TME microfluidic devices with magnetic beads. All chambers had magnetic beads, and the center chamber was loaded with F only matrix. Samples were either placed on a rotating magnet (Mag) or no magnet, stationary controls (No Mag). White dashed lines indicate interfaces of adjacent chambers. Scale bar = 500 μm. (b) Quantification of Hoescht positive area in side chambers normalized to Hoescht positive area in the middle chamber from experiment shown in part (a). (c) Representative images of Sytox dead cell staining of devices from (a); these images were taken on day 9 prior to fixation and staining for Ki67. (d) Quantification of dead cell count normalized to Hoescht count in each side chamber from experiment shown in (b). (e) Representative images of Ki67 staining of devices from (a). (f) Quantification of Ki67 positive area normalized to DAPI area in chambers with different matrix compositions from part (c). Note: images in (a) and (e) were collected at the same time point following fixation and staining; images in (c) are for same devices shown in (a) and (e) just taken at a different time. Data presented as average + SEM, n = 3 samples, *p < 0.05. Samples were compared using Kruskal-Walls followed by post-hoc Dunn's tests.

in CD44 activation further highlighting that HA binding alone may not cause enhanced receptor activation.

The OVCAR-8 WT cells had an increase in Src expression with concurrent Strain and PLT HA treatment compared to Strain treated NT (No HA) and SOL HA samples. We believe the deceased Src level in Strain treated WT cells compared to No Strain controls is a result of the highly dynamic and rapid turnover of Src in normal cells with studies reporting Src changes in shorter time frames (<20min).[58,59] While concurrent Strain and PLT HA treated shSCR cells had higher levels of Src compared to SOL HA and Strain groups, there was no difference compared to NT groups. This could be due to the role of Src as a mechanotransducer downstream of other signaling pathways, including integrin signaling.[60–62] Recent reports have suggested that CD44 and Src interactions are required for cytoskeletal regulation that drives ovarian cancer progression.[63] Notably, shCD44 cells demonstrated lower expression of Src when stimulated with both concurrent strain and PLT HA compared to non-strained controls; this suggests that high levels of CD44 may be necessary for strain-induced Src signaling in ovarian cancer cells. Our results show decreased expression of Src in shCD44 OVCAR-8 cells treated with 24 h Strain and PLT HA (Fig. 2b). The high levels of Src in the No Strain PLT HA samples may be due to other upstream regulators of Src that are HA-dependent such as RHAMM;[64] the fact that SOL HA samples did not show the same effect still supports our argument that synergistic effects occur through stromal HA and CD44 signaling in these cells. It is known that the ankyrin-binding domain of CD44 regulates Src family activity and can alter HA binding, suggesting bidirectional communication through mechanotransduction processes.[65,66] This could explain why our Strain and PLT HA samples have altered Src and ankyrin signaling in cells that express high levels of CD44. As CD44 is implicated in numerous signaling pathways, we hypothesize that the different stimulation combinations tested (i.e. - Strain + PLT HA vs. SOL HA) could differentially regulate separate downstream pathways. An example of this is previous work showing that Src activity is controlled through TGF-beta receptor interactions with strain. [67] In other words, additional studies are needed to define the specific mechanisms that govern the individual responses of Src and ankyrin after Strain stimulation in the context of the ovarian TME. In general, HA increases ankyrin in 2D studies for cells with high levels of CD44, and this phenomenon does not appear to be sensitive to strain stimulation (Fig. 2e).

Our studies expanded to quantify changes in ovarian cancer behaviors associated with disease progression. Specifically, we looked at proliferation as a stand-in for tumor growth, migration as a model of metastatic potential, and cell death as a readout of chemoresponse. CD44 has been associated with both migratory and proliferative behaviors in a variety of cell types, though previous studies have not reported strain-sensitivity of the receptor.[35,37,51] Additionally, sustained proliferative signaling is one of the hallmarks of cancer.[68] We explored both 2D and 3D models of the TME, focusing on SOL versus PLT or GEL HA as well as mechanical stimulation on Ki67 expression to measure proliferation of the cells. As we observed differences in proliferation rates between the WT, scramble and CD44 knockdown lines, we chose to complete our analyses based on data normalized to total cell count in each image. While this technique does not account for differences in metabolic states between the cell lines, such analyses are beyond the scope of the current study. OVCAR-8 WT and shSCR cells, that express high levels of CD44, demonstrated significant increases in proliferation with the PLT HA while SOL HA did not enhance proliferative behavior (Fig. 3b). The shCD44 cells did not exhibit increased proliferation with either type of HA stimulation. Moving into the 3D environment we also wanted to evaluate how a pre-treatment with tensile strain followed by with HA treatment would

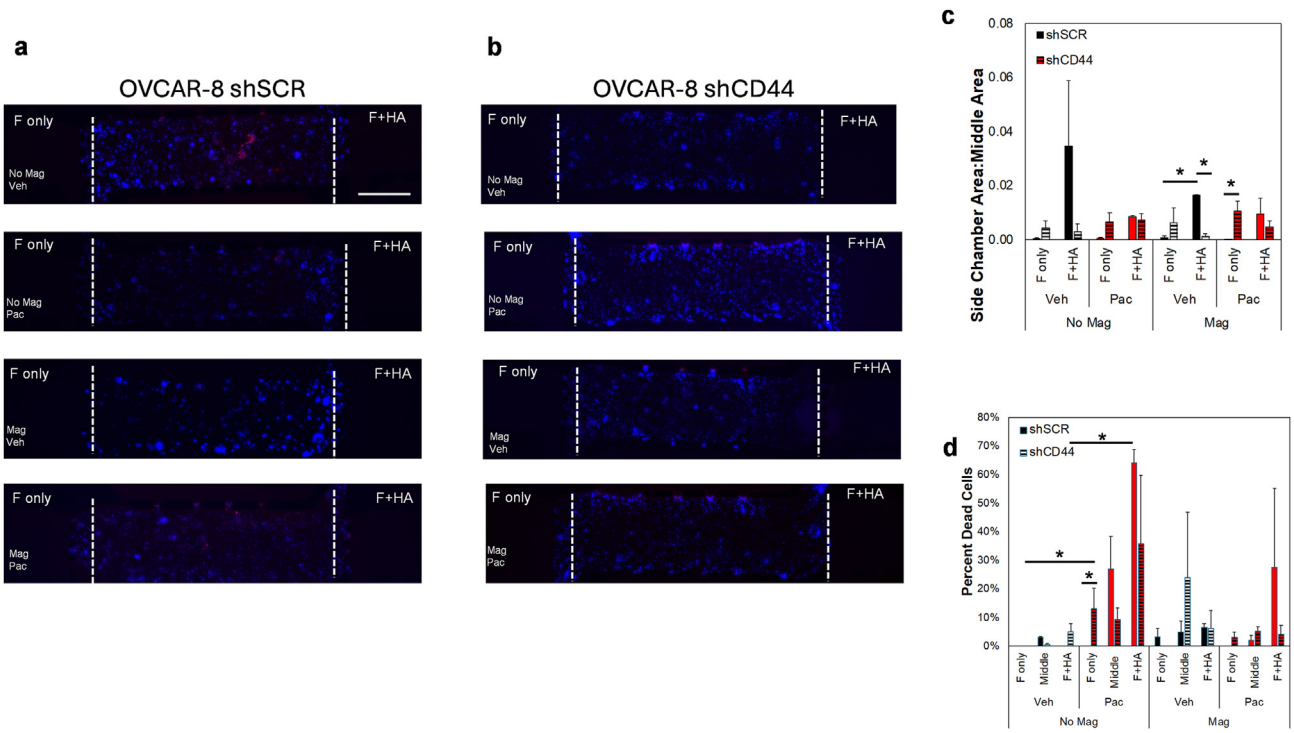

Fig. 7. CD44 Expression Regulates Migration Direction and Response to Pac with Concurrent Strain and GEL HA.(a) Representative images of Hoescht (blue) and Sytox dead cell (red) staining of OVCAR-8 shSCR cells cultured in 3-chamber TME microfluidic devices with magnetic beads. Samples were either placed on a rotating magnet (Mag) or no magnet, stationary controls (No Mag). White dashed lines indicate interfaces of adjacent chambers. Scale bar = 500 μm. (b) Representative images of Hoescht (blue) and Sytox dead cell (red) staining of OVCAR-8 shCD44 cells cultured in 3-chamber TME microfluidic devices with magnetic beads. Samples were either placed on a rotating magnet (Mag) or no magnet, stationary controls (No Mag). White dashed lines indicate interfaces of adjacent chambers. Scale bar = 500 μm. (c) Quantification of Hoescht positive area in side chambers normalized to Hoescht positive area in the middle chamber from experiment shown in part (a,b). (d) Quantification of dead cell count normalized to Hoescht count in each side chamber from experiment shown in (a,b). Data presented as average + SEM, n = 2 or 3 samples, *p < 0.05. Samples were compared using Kruskal-Walls followed by post-hoc Dunn's tests.

alter proliferative behaviors. The OVCAR-8 WT cells exhibited higher levels of Ki67 positive staining after Strain pre-treatment with the F + GEL HA treatment, while the shSCR cells demonstrated increased proliferation with F + GEL HA treatment both with and without the Strain pre-treatment (Fig. 3d). Notably, no difference in proliferation was observed in the no HA treatment (NT) samples of shCD44 cells compared to NT shSCR controls in 2D (Fig. 3); this suggests that in the absence of HA, the low expression of CD44 is not inhibitory of proliferation pathways in OVCAR-8 cells. Furthermore, there are minimal differences in proliferation between shSCR and shCD44 cells for 3D No Strain, F Only samples. This data suggests that CD44 is not the primary driver of proliferation for these cells under these specific conditions; this aligns with other studies that suggest several receptors, including epidermal growth factor, estrogen type b, and transforming growth factor receptors play a role in ovarian cancer proliferation.[69–71] However, Strain and F + GEL HA shSCR samples have higher proliferation than the same treatment shCD44 cells, supporting the idea that HA and strain synergistically signal in ovarian cancer cells to drive proliferation. While there was still some expression of CD44 in the shCD44 cells with Strain and F + GEL HA treatment (Fig. 1b), it was only ~33% versus shSCR of the same treatment. Overall, the data indicated that lowered CD44 expression decreased OVCAR-8 proliferation when treated with Strain and stromal-like HA. Even without HA, Strain treated OVCAR-8 WT and shSCR cells exhibited some increases in Ki67 staining, indicating that Strain can induce proliferation; this was not observed in the shCD44 samples. These results highlight that HA presentations that mimic the stromal HA (PLT HA in 2D or F + GEL HA in 3D) can increase ovarian cancer cell proliferation while models mimicking serum HA do not. Furthermore, the studies indicate that active strains can enhance the effect of stromal HA on CD44 signaling to increase proliferation of ovarian tumor cells.

The drug resistance studies show that a stromal-like presentation of HA can create a more drug resistant phenotype in the OVCAR-8 WT cells with Strain pre-treatment. This is observed by a lower cell death in the samples treated with Pac in an F + GEL HA matrix compared to the Veh treated group than those in the F Only matrix. The OVCAR-8 shCD44 samples have increased cell death in the Pac treated samples that received Strain pre-treatment in the F + GEL HA matrix versus the Veh controls, meaning the stromal-like presentation did not add the same level of protection. As a part of the generation of the shSCR and shCD44 lines, a selection module was included that using puromycin selection to generate the modified lines. It is possible that the machinery related to removing puromycin from the cells was activated when the samples were treated with Pac, potentially dampening the response to Pac regardless of Strain or HA exposure. The OVCAR-8 shSCR cells after Strain pre-treatment with Pac exhibit somewhat increased ankyrin levels but have larger increases in ankyrin levels in PLT HA samples compared to NT samples (Fig. 4f). As ankyrin is responsible for connecting the CD44 to the Rho-ROCK pathway, this could help explain increases in migration observed in the 3D TME models (Fig. 5d and e). In shCD44 samples, there is less ankyrin with PLT HA treatment for the Pac and Strain treated samples compared to Veh controls, suggesting that the CD44 receptor may play a role in strain and chemoresponse as it relates to regulation of the cytoskeleton. Finally, Pac treatment, regardless of Strain or HA treatment, did not significantly decrease proliferation in any of the cells tested. In WT cells especially, there seems to be larger increases in proliferation in Pac treated samples versus Veh samples that were cultured on PLT HA after Strain pre-treatment. Together with the Sytox data, this suggests that while Pac treatment does kill some cells, a more aggressive and still proliferative population remains following chemotherapy. This

could be one possible reason for the high rates of recurrent disease after treatment with traditional chemotherapies.

Finally, our studies utilized an advanced 3D TME model to investigate the interactions of strain and HA on ovarian cancer cell migration behaviors as a readout of metastatic potential. The microfluidic device design was chosen due to the 3 chambers that can be loaded independently, allowing for cellular components to be loaded into the middle while acellular gels with F Only or F + HA gels were loaded into the side chambers. The media flow pattern was chosen so that media was fed only into the middle chamber and allowed to diffuse into the side chambers; this resulted in a system were any secreted factors from cells loaded into the middle chamber equally diffused into the side chambers. Moreover, the feeding regime creates an equal magnitude of interstitial fluid flows towards the side chambers. Taken together, this means our studies controlled for both secreted factors and shear forces that could affect ovarian cancer cell migration and proliferation in the side chambers, solely focusing the studies on how HA in the TME drives cell behaviors. After 7 days, the OVCAR-8 WT and shSCR cells preferentially migrated into the side chambers containing the F + HA gel regardless of Strain pre-treatment (Fig. 5a,b,d,e). This was again observed when the cells were subject to continuous strain treatment with the Mag Strain experiment for 9 days (Figs. 6b and 7c). Interestingly, the shCD44 cells also migrated into the side chamber with F + GEL HA but only after Strain pre-treatment and only somewhat preferentially compared to F Only gels. Together, data from the 3D TME model may suggest that strain and HA signaling through CD44 alters migration and proliferation through different mechanisms, in line with what is known about phosphorylation of CD44 and the role of the receptor in directed migration. Recent work has shown that knockout of CD44 in mouse fibroblasts does not affect migratory capacity of the cells, only directionality.[49] The Strain pre-treatment did not have an influence on migration after 7 days in the 3D TME model. This may be explained by the delay between Strain treatment and final analyses of the devices, where any mechanical memory gained from the tensile strain treatment is dampened before the cells began to migrate.[72] As the strain is designed to mimic CAF-induced forces, future studies will focus on including these cells as an additional stromal component of the 3D TME model. However, CAFs were not included in the present study to eliminate CAF secreted factors and matrix remodeling as confounding factors when performing our studies. To differentiate between mechanical memory and concurrent Strain with HA exposure, we utilized a pseudo-cell system with magnetic beads in the 3D TME microfluidic model. In these devices, neither shSCR or shCD44 cells that received concurrent Mag Strain treatment responded to chemotherapy treatment (Fig. 7d). The shSCR samples responded to Pac treatment in and F + HA matrix with No Mag Strain, suggesting the mechanical stimulation is important in enhancing chemoresponse. Again, this alludes to the combined effects of mechanical strain and stromal-like presentation of HA creating an environment promotes tumor growth and inhibits a response to chemotherapy, potentially through CD44 signaling.

Overall, our studies included both concurrent Strain and HA as well as sequential Strain followed by HA treatments to study 3D TME models of ovarian cancer proliferation, migration, and response to Pac. Together, our results indicated that synergistic activities between stromal-like HA and Strain can promote enhanced CD44 activity related to these cellular behaviors. However, the same is not true for SOL HA, which mimics serum-like HA. Furthermore, we still see changes in Strain + GEL HA treatments in the sequential studies, where Pac treated followed Strain treatment. This may demonstrate a mechanical memory of the ovarian cancer cells, in line with prior work.[12,15] Together, this highlights the importance of 3D TME models for ovarian cancer that can study how mechanobiology regulates the disease progression and response to therapies.

5. Conclusions

In conclusion, CD44 expression, activation, and signaling is increased in ovarian cancer cells when stimulated with tensile strains and stromal-like HA but not necessarily serum-like HA. When HA was included in studies as a serum factor (SOL), we did not observe increases in CD44 signaling or cell proliferation, indicating that tension on the receptor when HA is embedded in the stroma may drive signaling in these cells. Ovarian cancer cells expressing high levels of CD44 have increased proliferation and migration with HA treatments that model stromal HA but not those that model serum HA. Finally, HA appears to be protective against paclitaxel treatment for cells that with CD44, while Strain is only somewhat protective in cells with lower levels of CD44. Together, our data suggests a unique interaction between mechanical stimulation and HA-binding that creates mechanosignaling through the CD44 receptor to drive ovarian cancer cell migration, proliferation, and chemoresponse.

Data availability

All data that support findings in this study are available from the corresponding author at reasonable request.

Ethical approval

This study does not contain studies with animal or human subjects performed by any of the authors.

CRediT authorship contribution statement

Maranda Kramer: Conceptualization, Data curation, Formal analysis, Investigation, Methodology, Writing – original draft. **Allyson Criswell:** Data curation, Formal analysis, Writing – original draft. **Kamari Marzette:** Data curation, Formal analysis, Writing – original draft. **Emerson Cutcliffe:** Data curation, Formal analysis, Writing – review & editing. **Mary Kathryn Sewell-Loftin:** Conceptualization, Data curation, Formal analysis, Funding acquisition, Investigation, Methodology, Resources, Supervision, Writing – original draft, Writing – review & editing.

Declaration of competing interest

M.K.S.L. receives compensation for consulting services from CerFlux, Incorporated. All other authors have no competing interests to declare.

Acknowledgements

The authors wish to thank the following funding sources: R00-CA230202 (M.K.S.L.), IMPACT Award (O'Neal Comprehensive Cancer Center, M.K.S.L.), the Fine Family Philanthropic Grant (M.K.S.L), UAB Blazer Fellowship (M.K.) and T32-EB023872 (M.K.).

Appendix A. Supplementary data

Supplementary data to this article can be found online at https://doi.org/10.1016/j.mbm.2024.100094.

References

1. Huang J, Chan WC, Ngai CH, et al. Worldwide burden, risk factors, and temporal trends of ovarian cancer: a global study. *Cancers (Basel)*. 2022;14(9).
2. Lisio MA, Fu L, Goyeneche A, Gao ZH, Telleria C. High-Grade serous ovarian cancer: basic sciences, clinical and therapeutic standpoints. *Int J Mol Sci*. 2019;20(4).
3. Doubeni CA, Doubeni AR, Myers AE. Diagnosis and management of ovarian cancer. *Am Fam Physician*. 2016;93(11):937–944.
4. Ricciardelli C, Ween MP, Lokman NA, Tan IA, Pyragius CE, Oehler MK. Chemotherapy-induced hyaluronan production: a novel chemoresistance mechanism in ovarian cancer. *BMC Cancer*. 2013;13:476.
5. Nishio S, Ushijima K. Clinical significance of primary debulking surgery and neoadjuvant chemotherapy-interval debulking surgery in advanced ovarian cancer. *Jpn J Clin Oncol*. 2020;50(4):379–386.
6. Vergote I, Trope CG, Amant F, et al. Neoadjuvant chemotherapy or primary surgery in stage IIIC or IV ovarian cancer. *N Engl J Med*. 2010;363(10):943–953.

7. Melamed A, Rauh-Hain JA, Gockley AA, et al. Association between overall survival and the tendency for cancer programs to administer neoadjuvant chemotherapy for patients with advanced ovarian cancer. *JAMA Oncol*. 2021;7(12):1782–1790.
8. Galluzzi L, Senovilla L, Vitale I, et al. Molecular mechanisms of cisplatin resistance. *Oncogene*. 2012;31(15):1869–1883.
9. Kramer M, Criswell A, Sewell-Loftin M. Biomaterial considerations for ovarian cancer models. *Frontiers in Materials*. 2023;10.
10. Monavarian M, Elhaw AT, Tang PW, et al. Emerging perspectives on growth factor metabolic relationships in the ovarian cancer ascites environment. *Semin Cancer Biol*. 2022;86(Pt 2):709–719.
11. Bregenzer ME, Horst EN, Mehta P, Novak CM, Repetto T, Mehta G. The role of cancer stem cells and mechanical forces in ovarian cancer metastasis. *Cancers (Basel)*. 2019;11(7).
12. Martinez A, Buckley M, Scalise CB, et al. Understanding the effect of mechanical forces on ovarian cancer progression. *Gynecol Oncol*. 2021;162(1):154–162.
13. Li SS, Ip CK, Tang MY, et al. Modeling ovarian cancer multicellular spheroid behavior in a dynamic 3D peritoneal microdevice. *J Vis Exp*. 2017;(120).
14. Asem M, Young A, Oyama C, et al. Ascites-induced compression alters the peritoneal microenvironment and promotes metastatic success in ovarian cancer. *Sci Rep*. 2020;10(1):11913.
15. Martinez A, Buckley MS, Scalise CB, et al. Utilization of a 3-D tissue engineered model to investigate the effects of perfusion on gynecologic cancer biology. *J Tissue Eng*. 2021;12:20417314211055015.
16. Sewell-Loftin MK, Bayer SVH, Crist E, et al. Cancer-associated fibroblasts support vascular growth through mechanical force. *Sci Rep*. 2017;7(1):12574.
17. Sewell-Loftin MK, Katz JB, George SC, Longmore GD. Micro-strains in the extracellular matrix induce angiogenesis. *Lab Chip*. 2020;(20):2776–2787.
18. Alcoser TA, Bordeleau F, Carey SP, et al. Probing the biophsyical properties of primary breast tumor-derived fibroblasts. *Cell Mol Bioeng*. 2015;8(1):76–86.
19. Bayer SV, Grither WR, Brenot A, et al. DDR2 controls breast tumor stiffness and metastasis by regulating integrin mediated mechanotransduction in CAFs. *Elife*. 2019;8:e45508.
20. Ansardamavandi A, Tafazzoli-Shadpour M. The functional cross talk between cancer cells and cancer associated fibroblasts from a cancer mechanics perspective. *Biochim Biophys Acta Mol Cell Res*. 2021;1868(11):119103.
21. Chen Y, McAndrews KM, Kalluri R. Clinical and therapeutic relevance of cancer-associated fibroblasts. *Nat Rev Clin Oncol*. 2021;18(12):792–804.
22. Oliveira-Ferrer L, Schmalfeldt B, Dietl J, Bartmann C, Schumacher U, Stürken C. Ovarian cancer-cell pericellular hyaluronan deposition negatively impacts prognosis of ovarian cancer patients. *Biomedicines*. 2022;10(11).
23. Anttila MA, Tammi RH, Tammi MI, Syrjanen KJ, Saarikoski SV, Kosma VM. High levels of stromal hyaluronan predict poor disease outcome in epithelial ovarian cancer. *Cancer Res*. 2000;60(1):150–155.
24. Tamada Y, Takeuchi H, Suzuki N, Aoki D, Irimura T. Cell surface expression of hyaluronan on human ovarian cancer cells inversely correlates with their adhesion to peritoneal mesothelial cells. *Tumour Biol*. 2012;33(4):1215–1222.
25. Kokoretsis D, Maniaki EK, Kyriakopoulou K, Koutsakis C, Piperigkou Z, Karamanos NK. Hyaluronan as "Agent Smith" in cancer extracellular matrix pathobiology: regulatory roles in immune response, cancer progression and targeting. *IUBMB Life*. 2022;74(10):943–954.
26. Price ZK, Lokman NA, Ricciardelli C. Differing roles of hyaluronan molecular weight on cancer cell behavior and chemotherapy resistance. *Cancers (Basel)*. 2018;10(12).
27. Turley EA, Noble PW, Bourguignon LY. Signaling properties of hyaluronan receptors. *J Biol Chem*. 2002;277(7):4589–4592.
28. Prevo R, Banerji S, Ferguson DJ, Clasper S, Jackson DG. Mouse LYVE-1 is an endocytic receptor for hyaluronan in lymphatic endothelium. *J Biol Chem*. 2001;276(22):19420–19430.
29. Lesley J, Hascall VC, Tammi M, Hyman R. Hyaluronan binding by cell surface CD44. *J Biol Chem*. 2000;275(35):26967–26975.
30. Noble PW, McKee CM, Cowman M, Shin HS. Hyaluronan fragments activate an NF-kappa B/I-kappa B alpha autoregulatory loop in murine macrophages. *J Exp Med*. 1996;183(5):2373–2378.
31. Rowley JE, Amargant F, Zhou LT, et al. Low molecular weight hyaluronan induces an inflammatory response in ovarian stromal cells and impairs gamete development in vitro. *Int J Mol Sci*. 2020;21(3).
32. Toole BP. Hyaluronan: from extracellular glue to pericellular cue. *Nat Rev Cancer*. 2004;4(7):528–539.
33. Bourguignon LY, Singleton PA, Zhu H, Diedrich F. Hyaluronan-mediated CD44 interaction with RhoGEF and Rho kinase promotes Grb2-associated binder-1 phosphorylation and phosphatidylinositol 3-kinase signaling leading to cytokine (macrophage-colony stimulating factor) production and breast tumor progression. *J Biol Chem*. 2003;278(32):29420–29434.
34. Bourguignon LY, Zhu H, Zhou B, Diedrich F, Singleton PA, Hung MC. Hyaluronan promotes CD44v3-Vav2 interaction with Grb2-p185(HER2) and induces Rac1 and Ras signaling during ovarian tumor cell migration and growth. *J Biol Chem*. 2001;276(52):48679–48692.
35. Chen L, Yao Y, Sun L, et al. Snail driving alternative splicing of CD44 by ESRP1 enhances invasion and migration in epithelial ovarian cancer. *Cell Physiol Biochem*. 2017;43(6):2489–2504.
36. Kim Y, Kumar S. CD44-mediated adhesion to hyaluronic acid contributes to mechanosensing and invasive motility. *Mol Cancer Res*. 2014;12(10):1416–1429.
37. Wolf KJ, Shukla P, Springer K, et al. A mode of cell adhesion and migration facilitated by CD44-dependent microtentacles. *Proc Natl Acad Sci U S A*. 2020;117(21):11432–11443.
38. Naor D, Sionov RV, Ish-Shalom D. CD44: structure, function, and association with the malignant process. *Adv Cancer Res*. 1997;71:241–319.
39. Kaufmann M, Heider KH, Sinn HP, von Minckwitz G, Ponta H, Herrlich P. CD44 variant exon epitopes in primary breast cancer and length of survival. *Lancet*. 1995;345(8950):615–619.
40. Begg CB, Rice MS, Zabor EC, Tworoger SS. Examining the common aetiology of serous ovarian cancers and basal-like breast cancers using double primaries. *Br J Cancer*. 2017;116(8):1088–1091.
41. Serio P, de Lima Pereira GF, Katayama MLH, Roela RA, Maistro S, Folgueira M. Somatic mutational profile of high-grade serous ovarian carcinoma and triple-negative breast carcinoma in young and elderly patients: similarities and divergences. *Cells*. 2021;10(12).
42. Lonning PE, Nikolaienko O, Pan K, et al. Constitutional BRCA1 methylation and risk of incident triple-negative breast cancer and high-grade serous ovarian cancer. *JAMA Oncol*. 2022;8(11):1579–1587.
43. Legg JW, Lewis CA, Parsons M, Ng T, Isacke CM. A novel PKC-regulated mechanism controls CD44 ezrin association and directional cell motility. *Nat Cell Biol*. 2002;4(6):399–407.
44. Herishanu Y, Gibellini F, Njuguna N, et al. CD44 Signaling via PI3K/AKT and MAPK/ERK pathways protects CLL cells from spontaneous and drug induced apoptosis through MCL-1. *Leuk Lymphoma*. 2012;52(9):11.
45. Gao Y, Foster R, Yang X, et al. Up-regulation of CD44 in the development of metastasis, recurrence and drug resistance of ovarian cancer. *Oncotarget*. 2015;6:9313–9326.
46. Koudelková L, Brábek J, Rosel D. Src kinase: key effector in mechanosignalling. *Int J Biochem Cell Biol*. 2021;131:105908.
47. Al-Rekabi Z, Fura AM, Juhlin I, Yassin A, Popowics TE, Sniadecki NJ. Hyaluronan-CD44 interactions mediate contractility and migration in periodontal ligament cells. *Cell Adh Migr*. 2019;13(1):138–150.
48. Mertsch S, Thanos S. Opposing signaling of ROCK1 and ROCK2 determines the switching of substrate specificity and the mode of migration of glioblastoma cells. *Mol Neurobiol*. 2014;49(2):900–915.
49. Razinia Z, Castagnino P, Xu T, Vazquez-Salgado A, Pure E, Assoian RK. Stiffness-dependent motility and proliferation uncoupled by deletion of CD44. *Sci Rep*. 2017;7(1):16499.
50. DeOre BJ, Partyka PP, Fan F, Galie PA. CD44 mediates shear stress mechanotransduction in an in vitro blood-brain barrier model through small GTPases RhoA and Rac1. *Faseb J*. 2022;36(5):e22278.
51. Hamann KJ, Dowling TL, Neeley SP, Grant JA, Leff AR. Hyaluronic acid enhances cell proliferation during eosinopoiesis through the CD44 surface antigen. *J Immunol*. 1995;154(8):4073–4080.
52. Levental KR, Yu H, Kass L, et al. Matrix crosslinking forces tumor progression by enhancing integrin signaling. *Cell*. 2009;139(5):891–906.
53. Tang YQ, Lee SA, Rahman M, Vanapalli SA, Lu H, Schafer WR. Ankyrin is an intracellular tether for TMC mechanotransduction channels. *Neuron*. 2020;107(4):759–761.
54. Kanungo J. Puromycin-resistant lentiviral control shRNA vector, pLKO.1 induces unexpected cellular differentiation of P19 embryonic stem cells. *Biochem Biophys Res Commun*. 2017;486(2):481–485.
55. Moran DM, Shen H, Maki CG. Puromycin-based vectors promote a ROS-dependent recruitment of PML to nuclear inclusions enriched with HSP70 and Proteasomes. *BMC Cell Biol*. 2009;10:32.
56. Goebeler M, Kaufmann D, Brocker EB, Klein CE. Migration of highly aggressive melanoma cells on hyaluronic acid is associated with functional changes, increased turnover and shedding of CD44 receptors. *J Cell Sci*. 1996;109(Pt 7):1957–1964.
57. Peck D, Isacke CM. Hyaluronan-dependent cell migration can be blocked by a CD44 cytoplasmic domain peptide containing a phosphoserine at position 325. *J Cell Sci*. 1998;111(Pt 11):1595–1601.
58. Liu M, Qin Y, Liu J, Tanswell AK, Post M. Mechanical strain induces pp60src activation and translocation to cytoskeleton in fetal rat lung cells. *J Biol Chem*. 1996;271(12):7066–7071.
59. Chaturvedi LS, Marsh HM, Basson MD. Src and focal adhesion kinase mediate mechanical strain-induced proliferation and ERK1/2 phosphorylation in human H441 pulmonary epithelial cells. *Am J Physiol Cell Physiol*. 2007;292(5):C1701–C1713.
60. Johnson BM, Johnson AM, Heim M, et al. Biomechanical stimulation promotes blood vessel growth despite VEGFR-2 inhibition. *BMC Biol*. 2023;21(1):290.
61. Lee HH, Tien SC, Jou TS, Chang YC, Jhong JG, Chang ZF. Src-dependent phosphorylation of ROCK participates in regulation of focal adhesion dynamics. *J Cell Sci*. 2010;123(Pt 19):3368–3377.
62. Block MR, Brunner M, Ziegelmeyer T, et al. The mechano-sensitive response of beta1 integrin promotes SRC-positive late endosome recycling and activation of Yes-associated protein. *J Biol Chem*. 2020;295(39):13474–13487.
63. Bourguignon LY, Wong G, Earle C, Krueger K, Spevak CC. Hyaluronan-CD44 interaction promotes c-Src-mediated twist signaling, microRNA-10b expression, and RhoA/RhoC up-regulation, leading to Rho-kinase-associated cytoskeleton activation and breast tumor cell invasion. *J Biol Chem*. 2010;285(47):36721–36735.
64. Savani RC, Liao J, Longoria C, et al. The hyaluronan receptor RHAMM is necessary for the activation of src kinase and the signaling pathway for endothelial nitric oxide production. *Faseb J*. 2016;30(S1):1204.11, 1204.11.
65. Bourguignon LY, Zhu H, Shao L, Chen YW. CD44 interaction with c-Src kinase promotes cortactin-mediated cytoskeleton function and hyaluronic acid-dependent ovarian tumor cell migration. *J Biol Chem*. 2001;276(10):7327–7336.
66. Zhu D, Bourguignon LY. The ankyrin-binding domain of CD44s is involved in regulating hyaluronic acid-mediated functions and prostate tumor cell transformation. *Cell Motil Cytoskelet*. 1998;39(3):209–222.

67. Hutcheson JD, Ryzhova LM, Setola V, Merryman WD. 5-HT(2B) antagonism arrests non-canonical TGF-beta 1-induced valvular myofibroblast differentiation. *J Mol Cell Cardiol*. 2012;53(5):707–714.
68. Hanahan D, Weinberg RA. Hallmarks of cancer: the next generation. *Cell*. 2011; 144(5):646–674.
69. Sewell JM, Smyth JF, Langdon SP. Role of TGF alpha stimulation of the ERK, PI3 kinase and PLC gamma pathways in ovarian cancer growth and migration. *Exp Cell Res*. 2005;304(1):305–316.
70. Schuler-Toprak S, Moehle C, Skrzypczak M, Ortmann O, Treeck O. Effect of estrogen receptor beta agonists on proliferation and gene expression of ovarian cancer cells. *BMC Cancer*. 2017;17(1):319.
71. Hudson LG, Zeineldin R, Silberberg M, Stack MS. Activated epidermal growth factor receptor in ovarian cancer. *Cancer Treat Res*. 2009;149:203–226.
72. Yang C, Tibbitt MW, Basta L, Anseth KS. Mechanical memory and dosing influence stem cell fate. *Nat Mater*. 2014;13(6):645–652.